Stable and simple quantitative phase contrast imaging by Fresnel biprism

Samira Ebrahimi,[1] Masoomeh Dashtdar,[1, a)] Emilio Sánchez-Ortiga,[2] Manuel Martínez-Corral,[2] and Bahram Javidi[3]

[1)] *Faculty of Physics, Shahid Beheshti University, Evin, Tehran 19839-69411, Iran*

[2)] *3D Imaging and Display Laboratory, Department of Optics, University of Valencia, E-46100 Burjassot, Spain*

[3)] *Department of Electrical and Computer Engineering, University of Connecticut, Storrs, Connecticut 06269-4157, USA*

Digital holographic (DH) microscopy has grown into a powerful nondestructive technique for real-time study of living cells including dynamic membrane changes and cell fluctuations in nanometer and sub-nanometer scales. The conventional DH microscopy configurations require a separately generated coherent reference wave that results in a low phase stability and a necessity to precisely adjust the intensity ratio between two overlapping beams. In this work, we present a compact, simple and very stable common-path DH microscope, employing a self-referencing configuration. The microscope is implemented by a diode laser as the source and a Fresnel biprism for splitting and recombining the beams simultaneously. In the overlapping area, linear interference fringes with high contrast are produced. The frequency of the interference pattern could be easily adjusted by displacement of the biprism along the optical axis without decrease in fringe contrast. To evaluate the validity of the method, the spatial noise and temporal stability of the setup are compared with the common off-axis DH microscope based on Mach-Zehnder interferometer (MZI). It is shown that the proposed technique has low mechanical noise as well as superb temporal stability with sub-nanometer precision without any external vibration isolation. The higher temporal stability improves the capabilities of the microscope for studying micro-objects fluctuations, particularly in the case of biological specimens. Experimental results are presented using red blood cells (RBCs) and silica microspheres to demonstrate the system performance.

PACS numbers: 42.30.Rx, 42.40.Kw, 42.62.Be, 87.15.Ya

Quantitative phase imaging (QPI) is an efficient method that enables to record the entire complex optical wavefront of object relying on the principle of interferometry.[1–3] Digital holographic (DH) microscopy is a non-destructive QPI method for investigating the optical thickness of the specimen as well as the nanometric variations of the surface using the phase information extracted from numerical phase retrieval algorithms.[4–7] Since the membrane fluctuation of living cells is highly correlated with their health status, DH microscopy is of interest for a wide range of applications in medicine and biology.[8–15]

On-axis configuration as the simplest arrangement in DH microscopy provides the reconstructed images with high resolution.[16,17] However, overlap between zero order and object wave in angular spectrum makes it difficult to retrieve correct phase information from only a single hologram.[18,19] Besides, Off-axis geometry by superimposing two slightly tilted light beams, enables the separation of sample information from zero spatial frequencies without using phase shifting operations.[20,21] Hence, the method can be applied to monitor dynamical changes of the optical path length in media such as living cells.[22,23] The most conventional off-axis configurations are two-beam DH microscopy (TBDHM) setups which are based on Michelson and Mach-Zehnder interferometer (MZI) geometries. In these methods, light travels through two different paths, one modulated by the sample and the other acting as a reference. However, this configurational complexity causes low-temporal phase stability due to vibration of several optical elements. Temperature gradient, air perturbations, and other environmental effects in two arms of the interferometer could also lead to higher noise.

To overcome the mentioned shortcoming, recently several common-path DH microscopy configurations have been proposed based on self-referencing geometry in which a portion of the object beam containing only cell media is used as the reference.[24–32] The natural inquiry that arises is whether one can design a more precise common-path configuration that takes advantage of the on-axis method in simplicity and stability while benefiting from the single-shot imaging ability of the off-axis method.

In this work, we describe the development of a DH microscopy system in which the interferograms are acquired only by a Fresnel biprism. Fresnel biprism has recently been used in super-resolution imaging by structured illumination,[33] high-contrast incoherent interferometry,[34] phase-shifting microscopy[35] and interference electron microscopy.[36] Here, the phase imaging capability of the biprism is of interest. Similar to the on-axis setups, the proposed method is very simple and compact due to the removal of additional optical components, e.g. mirrors, beamsplitters and neutral density filters. Easy implementation without any requirement for precise alignment makes it suitable for integration with many configurations in real-time measurements. The main advantage of the technique is its high stability as a result of strong phase correlation during mechanical vibration. This leads to the reduction of mechanical noise and discards the requirement of positioning the setup on an optical vibration-isolation table. Moreover, the interferometer is able to produce the variable frequency of linear fringes with high contrast through the precise adjustment of the intensity ratio between two inter-

[a)] Electronic mail: m-dashtdar@sbu.ac.ir

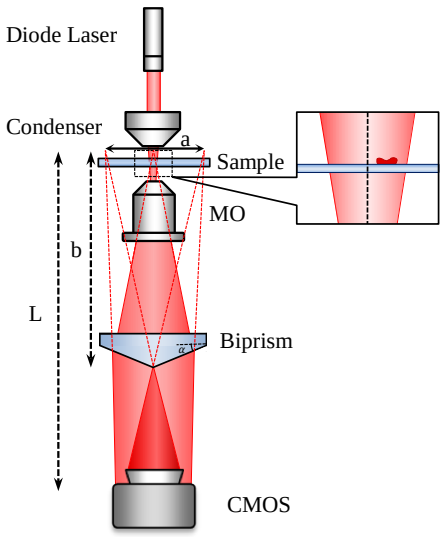

Figure 1. Experimental setup of self-referencing DH microscopy by biprism configuration. The right box in the figure displays the magnified part of the setup which is shown by dashed line square. Half of the optical field of view acts as the reference of the other half.

fered beams.

The schematic configuration of the biprism interferometer (BI) setup is illustrated in Fig. 1. A diode laser having maximum output power of 2 mW with the wavelength $\lambda = 650$ nm and 5 mm coherence length is used as the source. The parallel beam of light enters an inverted microscope and illuminates the sample under investigation by a condenser lens (E Plan, NA= 0.25). The sample which is positioned in the half of the illuminated spot (see inset of Fig. 1) is magnified by a microscope objective (MO) (E Plan, 40×, NA= 0.65). After passing through the MO, the object beam meets the Fresnel biprism where the wavefront splits into two overlapping beams creating off-axis geometry. The biprism is constructed from BK7 glass and has a refringence angle $\alpha = 0.02$ radian, and a refractive index $n = 1.51$. The linear interference fringes are recorded by a CMOS sensor (Point Grey BFLY-U3-23S6M-C, 8 bit dynamic range, 5.86 μm pixel pitch) located at the magnified image plane and have an equal spacing,[37]

$$d = \frac{L\lambda}{b(n-1)\alpha}, \tag{1}$$

where L and b are the distances from the virtual sources to the sensor plane and the biprism, respectively, as depicted in Fig. 1. Figures 2(a-c) represent that the period of recorded interference fringes increases by decreasing the distance b while keeping L constant, as expected from Eq. 1. That being so, adjustment of the fringes period can be easily performed just through displacement of the biprism along the optical axis. It is worth mentioning that the intensity ratios as well as the optical path lengths of the two beams are the same for different spatial frequencies, providing high-contrast interference fringes. The field of view is chosen so that the effect of the biprism central edge diffraction is excluded.

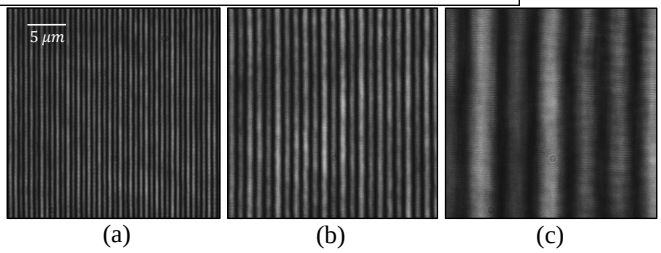

Figure 2. Spatial frequency variation of interference fringes by displacement of biprism along the optical axis for (a) $b = 28$ cm, (b) $b = 15$ cm, (c) $b = 4$ cm. All holograms are recorded at $L = 30$ cm.

Thin smears of red blood cells (RBCs) are considered as the samples in our study. Figure 3(a) represents the recorded hologram of a single RBC. Since the recording plane of the hologram is located near the focused image plane, the holograms are numerically reconstructed using angular spectrum propagation approach in which the intensity and phase information of object could be reconstructed at the image plane by propagating the angular spectrum of object filtered from the Fourier transform of the complex amplitude (see Ref. 38 for thorough description of the method). For phase compensation and obtaining the phase profile of the sample, two holograms in the presence and absence of the object are recorded and reconstructed separately. By subtracting their reconstructed phase images, the wrapped phase profile of the object is acquired. The continuous phase distribution is retrieved by Goldstein's branch-cut method.[39] In this way, the reconstructed intensity (Fig. 3(b)) and phase distributions of the RBC (Fig. 3(c)) are achieved. By considering the average refractive index of RBC ($n_{rbc} = 1.41$) and the blood plasma ($n_{bp} = 1.34$) as surrounding environment,[40] the quantitative thickness image of RBC (Δd) is obtained from the reconstructed phase distribution ($\Delta\phi$) by

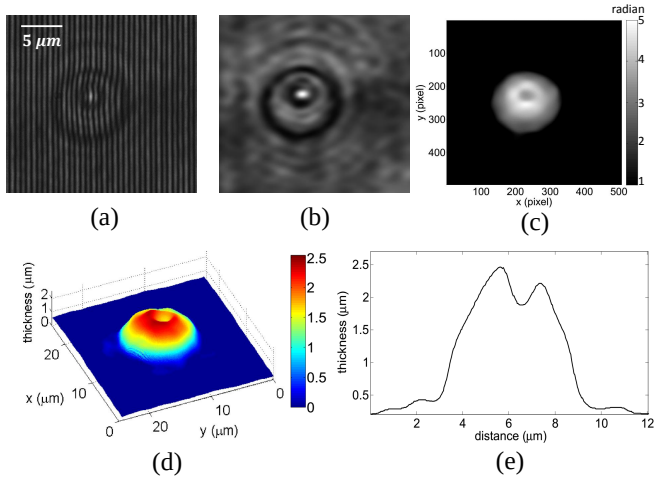

Figure 3. (a) Recorded hologram of the RBC, (b) reconstructed intensity, (c) obtained continuous phase image after phase unwrapping, (d) calculated thickness profile, and (e) diagonal cross-section of the thickness distribution.

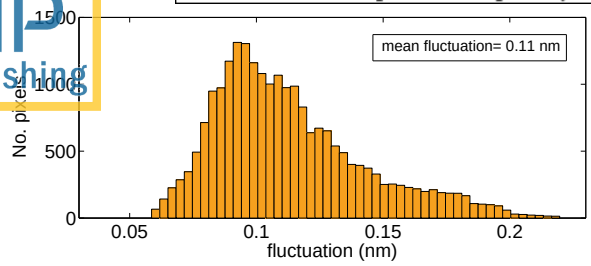

Figure 4. Histogram of standard deviation of the setup fluctuations. The fluctuations of 150×150 pixels are detected for 60 seconds at a frame rate of 41 Hz without vibration isolation.

$\Delta d = \lambda \Delta\phi / [2\pi(n_{rbc} - n_{bp})]$. The results of calculated thickness distributions, depicted in Figs. 3(d,e), signify the normal biconcave shape of RBC, and thus confirm the reliability of the method.

To survey the temporal stability of the technique, holograms are recorded at the rate of 41 Hz for 60 seconds, while a blank slide is placed in the sample position. The temporal path length variations are determined by selecting an area of 150×150 pixels. The fluctuation at each pixel is measured by calculating the standard deviation of path length changes. The mean of these fluctuations, presented in Fig. 4, can be considered as a measure of temporal stability of the method which is 0.11 nm without any vibration isolation. Such sub-nanometer temporal stability introduced by common-path geometry, makes our method a promising candidate for investigation of time-evolving, short-amplitude fluctuations with high accuracy. We record the holograms of a single RBC for 6 seconds at the frequency of 41 Hz. The fluctuation maps of RBC membrane for each second, shown in Fig. 5, signify variations in the order of a few tens of nanometers which are evidently concentrated both in the edge and center parts due to slight translations and high-frequency dynamic domains within the cell. Such subdomains of RBC have been studied by popescu *et al.* using a Fourier phase microscopy method.[40]

To analyse the validity of the proposed method, we compare our results with those extracted from conventional TBDHM

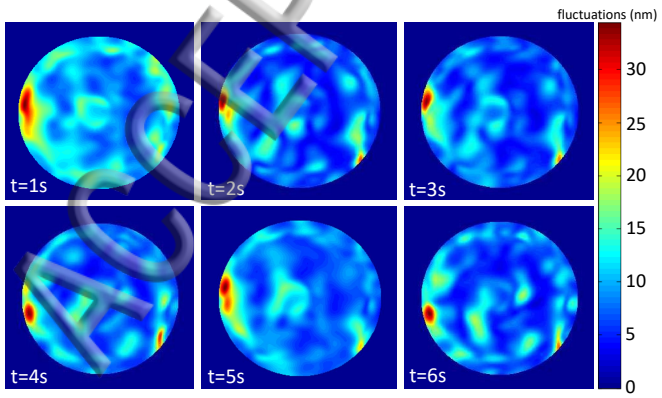

Figure 5. Temporal evolution of RBC membrane fluctuations. Holograms are recorded at a frame rate of 41 Hz by BI configuration.

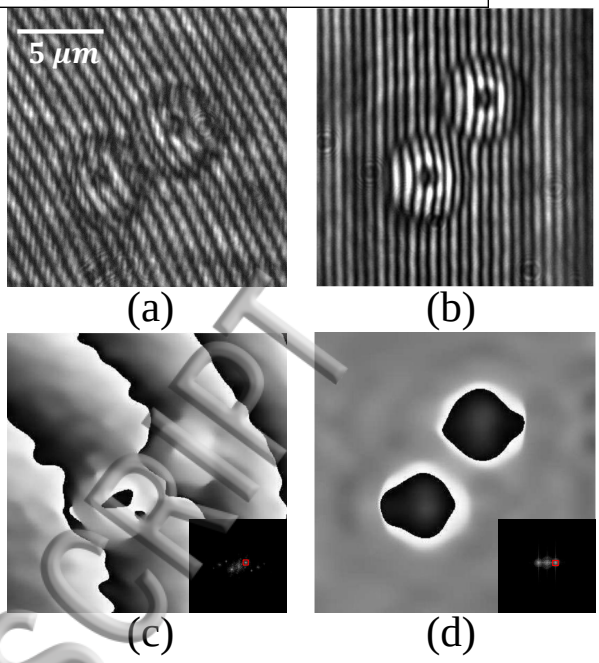

Figure 6. (a) and (b): holograms of silica microspheres obtained by TBDHM and BI configurations, respectively. (c) and (d): the reconstructed phase distributions of (a) and (b) obtained by filtering the inset power spectra using a 19×19 pixel window filter. (b-c) have the same pixel resolution as (a).

based on MZI technique. Since the optical path difference between the two arms of TBDHM is more than the coherence length of the diode laser, a He-Ne laser (Thorlabs, 632.8 nm, 5 mW) is used as the coherent light source. Silica microspheres (4.47-μm diameter) were used as the standard phase samples for comparison of two methods. Figures. 6(a,b) show the recorded holograms of the microspheres by TBDHM and BI configurations, respectively. In the reconstruction process, by isolating the image angular spectra in Fourier domain using an equal rectangular window for both methods (see the insets in Figs. 6(c,d)) and applying an inverse Fourier transformation, wrapped phase distributions of microspheres are retrieved from the wavefront complex amplitudes. Defocusing effect induced by flowing the cells through the microscope cell could be compensated numerically by propagating the spectrum of object to the best focus reconstruction plane determined by an auto-focusing algorithm.[41] As both superimposing tilted beams in BI geometry have the same wavefront curvature, the quadratic phase factor is removed (Fig. 6(d)), but it clearly remains in TBDHM phase pattern of Fig. 6(c). To compensate this effect, the achieved phase image of a reference hologram is subtracted from the sample phase distribution. However, because of individual vibration of the optical components in two arms of the interferometer, the phase factor could not be completely eliminated, and thus the reconstruction of the precise spatial phase information of the sample is not possible. The retrieved intensity distributions of microspheres for TBDHM and BI methods and their associated unwrapped phase profiles are shown in Fig.7 which indicate that

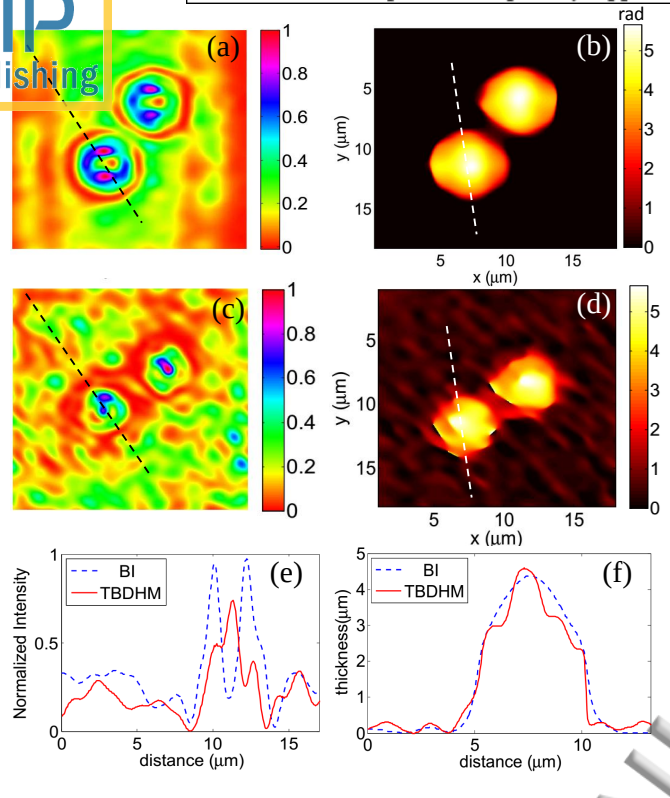

Figure 7. (a) Intensity and (b) continuous phase distribution of silica microspheres using BI, (c) intensity and (d) continuous phase distribution of the microspheres using TBDHM. Cross-sections of (e) intensity and (f) thickness distributions along the dashed lines for two methods.

the spatial noise level in TBDHM is much higher in both intensity and phase. In addition to the outlined phase factor, any defects, aberrations, and ghost images, introduced by the optical elements, give rise to periodic patterns with frequencies near the hologram fringes which cause additional errors. Crucially, the high spatial frequencies (equivalent to the fine structural details including sharp edges) which are suppressed in TBDHM configuration due to vibration, are recovered in BI configuration (see Fig. 7(e)). Moreover, the influence of spatial noise on the cross-section of microsphere thickness distribution in TBDHM technique is obviously larger than that observed in BI method, according to the Fig. 7(f).

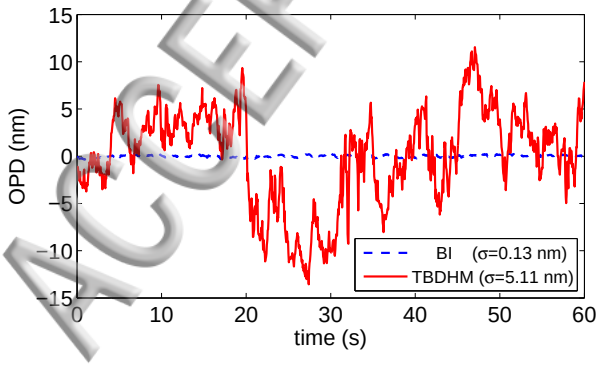

Figure 8. The temporal variation of optical path delay in an area of 4×4 pixels for both BI and TBDHM methods. σ is the standard deviation of the optical path length difference.

The temporal stability of two approaches is also compared. The time evolutions of optical path difference of background in an area of 4×4 pixels (related to approximately a diffraction limited spot) are shown in Fig. 8 for a period of 60 seconds with a rate of 18 Hz without vibration isolation. The standard deviation of temporal variations for BI configuration is about 0.13 nm which indicates that its stability is approximately forty times better than TBDHM method (5.11 nm). It demonstrates a clear-cut evidence of high robustness and ability of the proposed technique to measure sub-nanometer morphological changes which could be a potential parameter in medicine diagnosis.[24,42]

In conclusion, we have implemented a common-path DH microscopy setup by the use of a Fresnel biprism which enables us to obtain significant phase information of low contrast micron-sized samples such as living cells. The setup is very compact, cost-effective and easy to implement. It could be applied to many existing conventional optical microscopes which use a low-cost diode laser as a source, simply by adding a biprism. Remarkably, the advantage of the proposed technique is sub-nanometer temporal stability that is measured as 0.11 nm, without any vibration isolation. Precise adjustment of the intensity ratio between object and reference beams even without accurate alignment of the biprism leads to the high contrast of fringes. Additionally, since the period of fringes depends solely on the axial position of the biprism, frequency adjustment can be easily performed which assists in studying the micro-objects with different sizes and shapes. The method is employed to determine membrane fluctuations of red blood cells which are on the order of tens of nanometers. The comparison between the presented technique and the conventional DH microscopy setup based on MZI reveals that our proposal has less spatial noise and higher temporal stability.

Acknowledgements.— M.D. and S.E. were supported by the Iran National Science Foundation (INSF).

REFERENCES

[1] W. Choi, C. Fang-Yen, K. Badizadegan, S. Oh, N. Lue, R. R. Dasari, and M. S. Feld, Nature Methods **4**, 717 EP (2007).
[2] N. Lue, J. W. Kang, T. R. Hillman, R. R. Dasari, and Z. Yaqoob, Applied Physics Letters **101**, 084101 (2012).
[3] K. Lee, K. Kim, J. Jung, J. Heo, S. Cho, S. Lee, G. Chang, Y. Jo, H. Park, and Y. Park, Sensors **13**, 4170 (2013).
[4] J. W. Goodman and R. W. Lawrence, Applied Physics Letters **11**, 77 (1967).
[5] U. Schnars and W. P. O. Jüptner, Measurement Science and Technology **13**, R85 (2002).
[6] P. Ferraro, S. D. Nicola, A. Finizio, G. Pierattini, and G. Coppola, Applied Physics Letters **85**, 2709 (2004).
[7] M. K. Kim, "Digital holographic microscopy," in *Digital Holographic Microscopy: Principles, Techniques, and Applications* (Springer New York, New York, NY, 2011) pp. 149–190.
[8] P. Marquet, B. Rappaz, P. J. Magistretti, E. Cuche, Y. Emery, T. Colomb, and C. Depeursinge, Opt. Lett. **30**, 468 (2005).
[9] B. Rappaz, P. Marquet, E. Cuche, Y. Emery, C. Depeursinge, and P. J. Magistretti, Opt. Express **13**, 9361 (2005).

[10] B. Kemper and G. von Bally, Appl. Opt. **47**, A52 (2008).
[11] Y. Jang, J. Jang, and Y. Park, Opt. Express **20**, 9673 (2012).
[12] I. Bianco, M. Paturzo, O. Gennari, A. Finizio, and P. Ferraro, Opt. Express **21**, 23985 (2013).
[13] N. Pavillon, J. Kühn, C. Moratal, P. Jourdain, C. Depeursinge, P. J. Magistretti, and P. Marquet, PLOS ONE **7**, 1 (2012).
[14] F. Merola, L. Miccio, M. Paturzo, A. Finizio, S. Grilli, and P. Ferraro, Opt. Lett. **36**, 3079 (2011).
[15] A. Doblas, E. Roche, F. J. Ampudia-Blasco, M. Martínez-Corral, G. Saavedra, and J. Garcia-Sucerquia, Journal of Microscopy **261**, 285 (2016).
[16] D. Gabor, Nature **161**, 777 EP (1948).
[17] C. Fournier, L. Denis, and T. Fournel, J. Opt. Soc. Am. A **27**, 1856 (2010).
[18] J. Garcia-Sucerquia, W. Xu, S. K. Jericho, P. Klages, M. H. Jericho, and H. J. Kreuzer, Appl. Opt. **45**, 836 (2006).
[19] V. Micó, L. Granero, Z. Zalevsky, and J. García, Journal of Optics A: Pure and Applied Optics **11**, 125408 (2009).
[20] E. Cuche, F. Bevilacqua, and C. Depeursinge, Opt. Lett. **24**, 291 (1999).
[21] M. Liebling, T. Blu, and M. Unser, J. Opt. Soc. Am. A **21**, 367 (2004).
[22] F. Dubois, C. Yourassowsky, O. Monnom, J.-C. Legros, O. Debeir, P. Van Ham, R. Kiss, and C. Decaestecker, Journal of biomedical optics **11**, 054032 (2006).
[23] I. Moon, F. Yi, and B. Rappaz, Appl. Opt. **55**, A86 (2016).
[24] B. Kemper, A. Vollmer, C. E. Rommel, J. Schnekenburger, and G. von Bally, Journal of Biomedical Optics **16**, 026014 (2011).
[25] N. T. Shaked, Opt. Lett. **37**, 2016 (2012).
[26] P. Ferraro, D. Alferi, S. D. Nicola, L. D. Petrocellis, A. Finizio, and G. Pierattini, Opt. Lett. **31**, 1405 (2006).
[27] P. Bon, G. Maucort, B. Wattellier, and S. Monneret, Opt. Express **17**, 13080 (2009).
[28] J. Di, Y. Li, M. Xie, J. Zhang, C. Ma, T. Xi, E. Li, and J. Zhao, Appl. Opt. **55**, 7287 (2016).
[29] V. Chhaniwal, A. S. G. Singh, R. A. Leitgeb, B. Javidi, and A. Anand, Opt. Lett. **37**, 5127 (2012).
[30] S. Ebrahimi, A.-R. Moradi, A. Anand, and B. Javidi, Opt. Lett. **39**, 2916 (2014).
[31] A. Anand, A. Faridian, V. K. Chhaniwal, S. Mahajan, V. Trivedi, S. K. Dubey, G. Pedrini, W. Osten, and B. Javidi, Applied Physics Letters **104**, 103705 (2014).
[32] S. Mahajan, V. Trivedi, P. Vora, V. Chhaniwal, B. Javidi, and A. Anand, Opt. Lett. **40**, 3743 (2015).
[33] E. Sánchez-Ortiga, M. Martínez-Corral, G. Saavedra, and J. Garcia-Sucerquia, Opt. Lett. **39**, 2086 (2014).
[34] A. Doblas, G. Saavedra, M. Martínez-Corral, J. C. Barreiro, E. Sanchez-Ortiga, and A. Llavador, J. Opt. Soc. Am. A **30**, 140 (2013).
[35] J. Endo, J. Chen, D. Kobayashi, Y. Wada, and H. Fujita, Appl. Opt. **41**, 1308 (2002).
[36] G. F. Missiroli, G. Pozzi, and U. Valdre, Journal of Physics E: Scientific Instruments **14**, 649 (1981).
[37] E. Hecht, *Optics* (ADDISON WESLEY Publishing Company Incorporated, 2016).
[38] A. Anand, V. K. Chhaniwal, and B. Javidi, J. Display Technol. **6**, 500 (2010).
[39] B. Gutmann and H. Weber, Appl. Opt. **39**, 4802 (2000).
[40] G. Popescu, K. Badizadegan, R. R. Dasari, and M. S. Feld, Journal of Biomedical Optics **11**, 040503 (2006).
[41] P. Langehanenberg, B. Kemper, D. Dirksen, and G. von Bally, Appl. Opt. **47**, D176 (2008).
[42] Y. Kim, H. Shim, K. Kim, H. Park, S. Jang, and Y. Park, Sci Rep **4**, 6659 (2014).

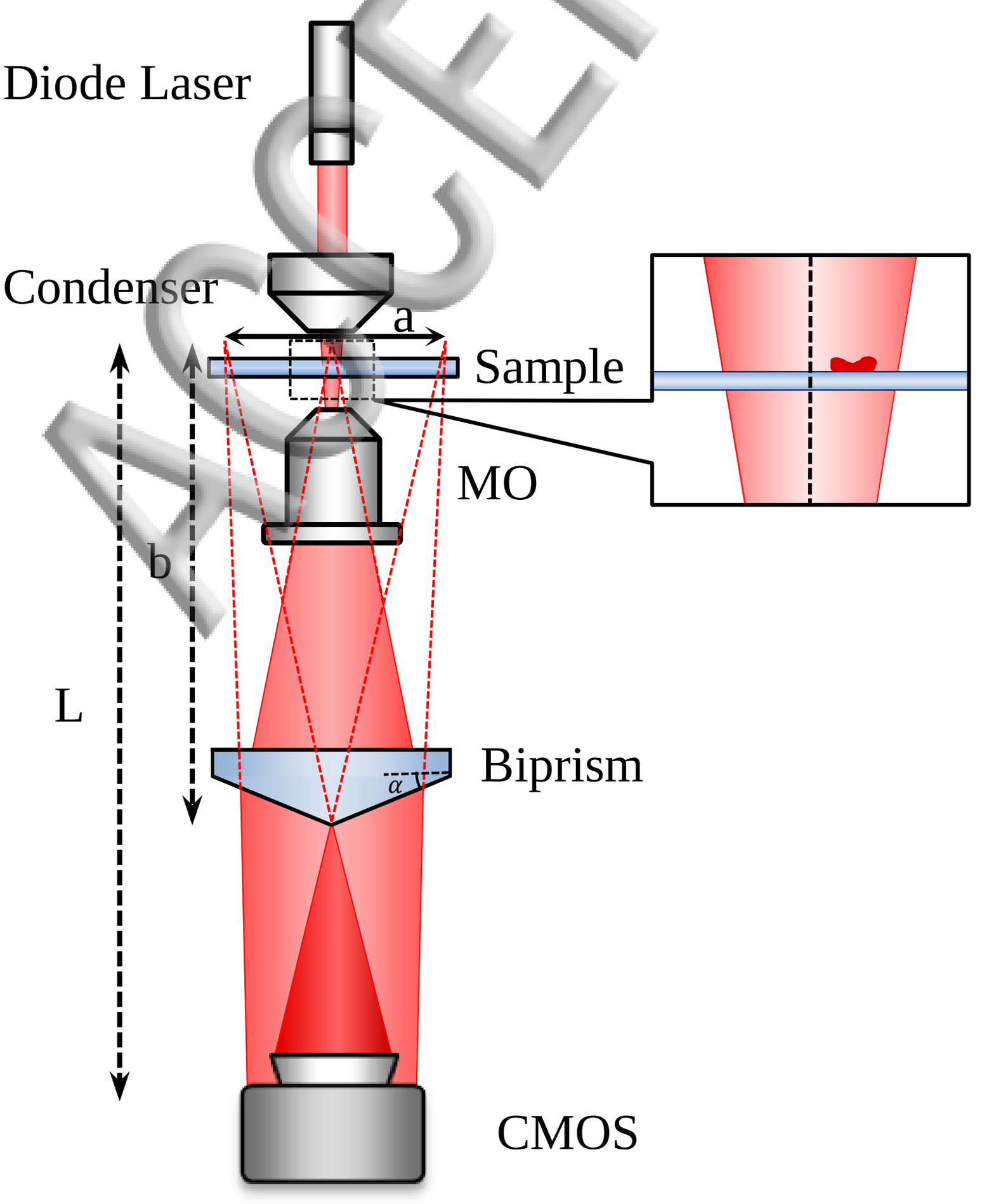
Diode Laser
Condenser
a
Sample
MO
b
L
Biprism
α
CMOS

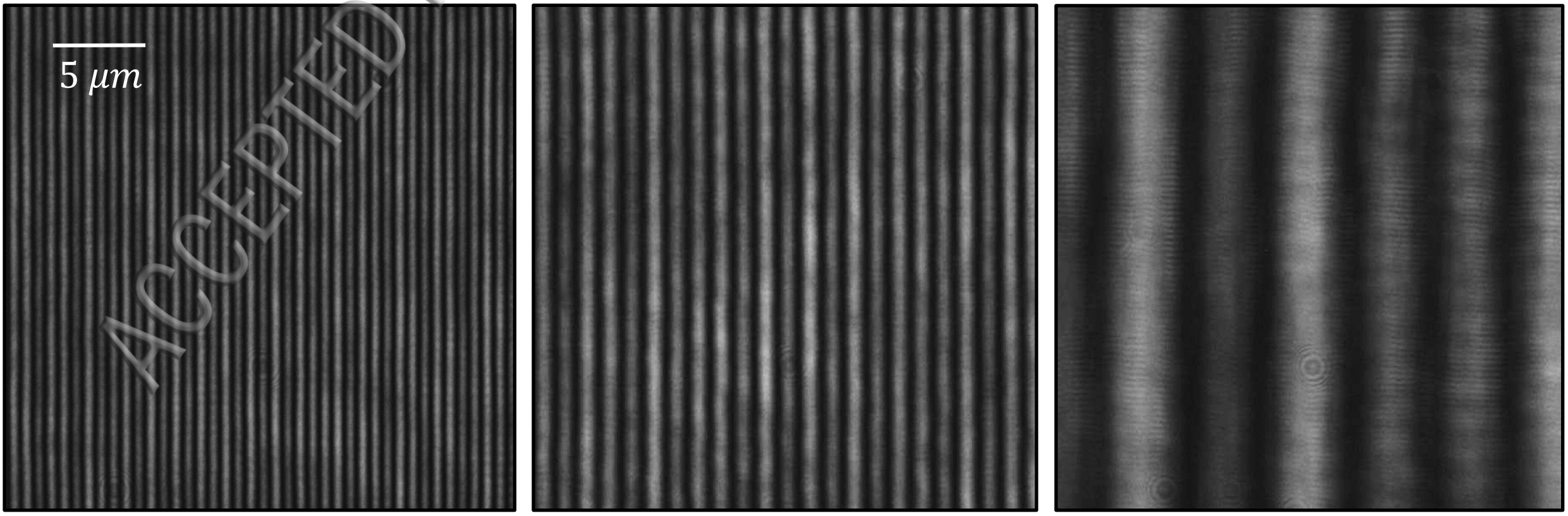

(a) (b) (c)

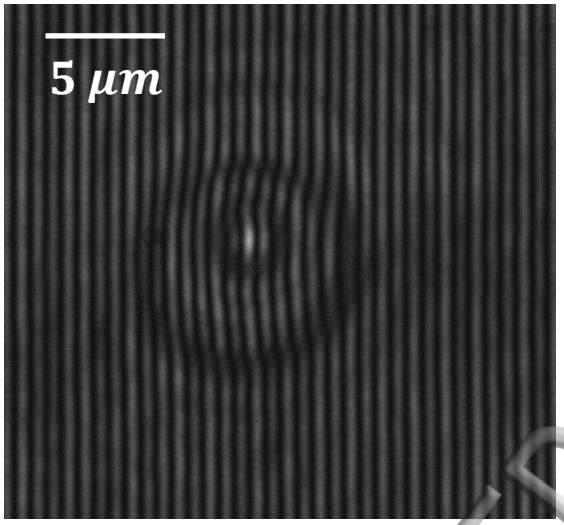

(a)

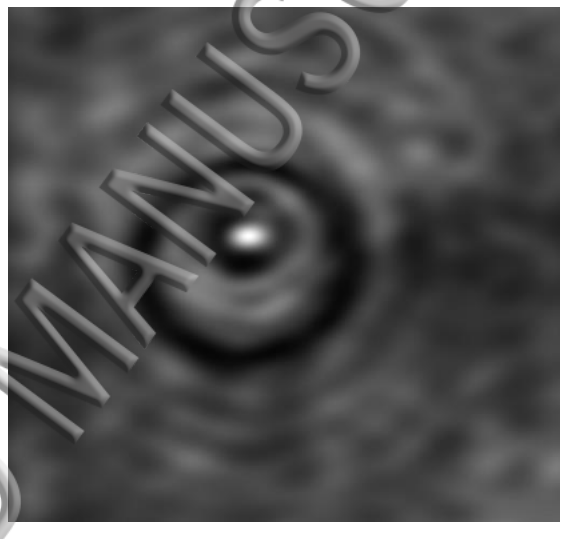

(b)

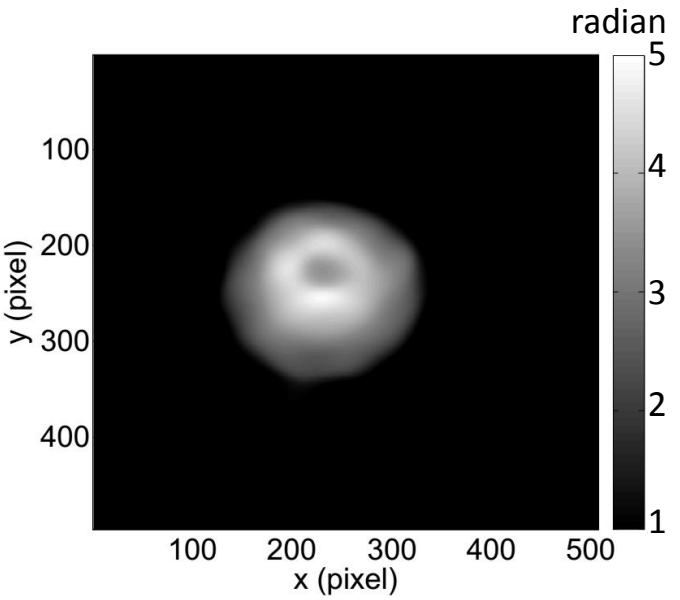

(c)

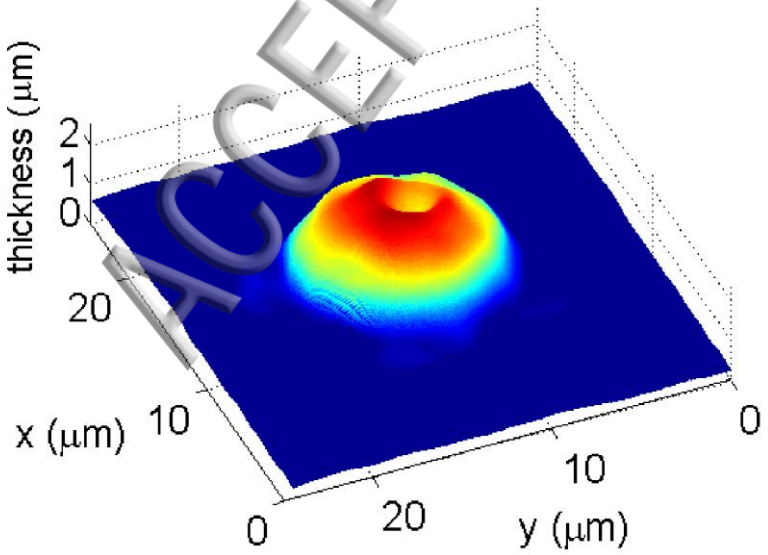

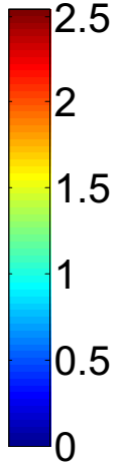

(d)

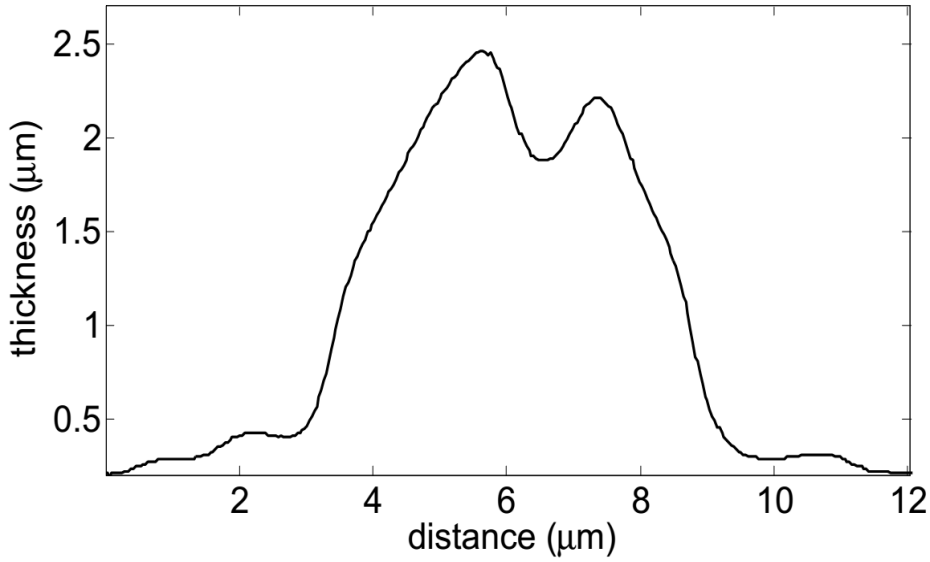

(e)

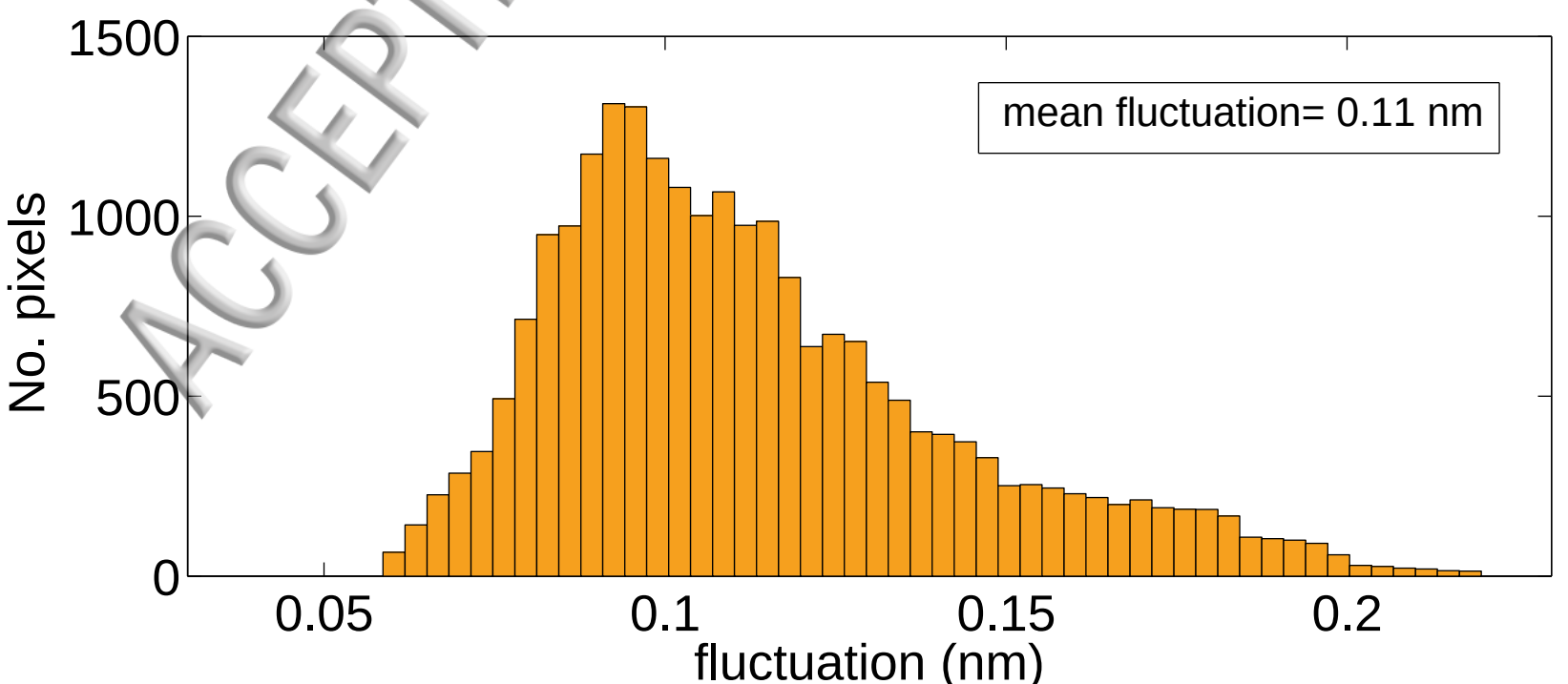
mean fluctuation= 0.11 nm
No. pixels
fluctuation (nm)
0
500
1000
1500
0.05
0.1
0.15
0.2

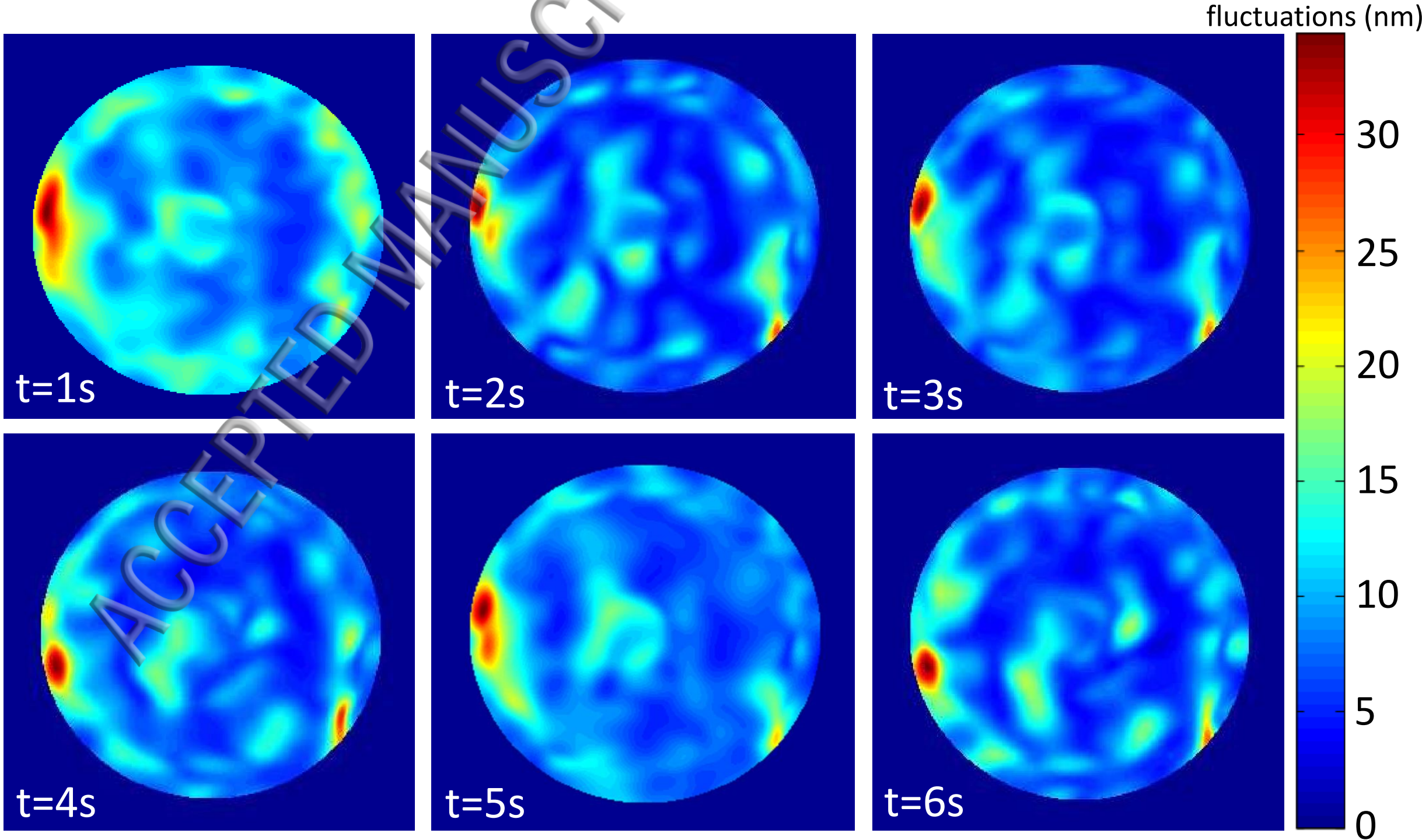

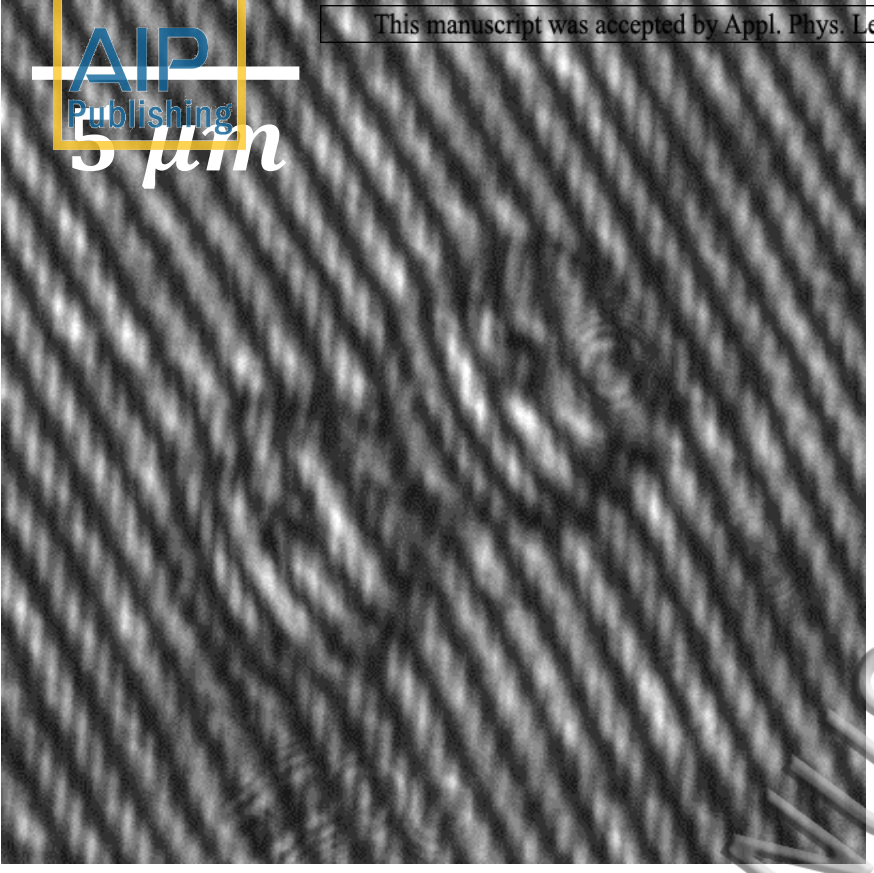

(a)

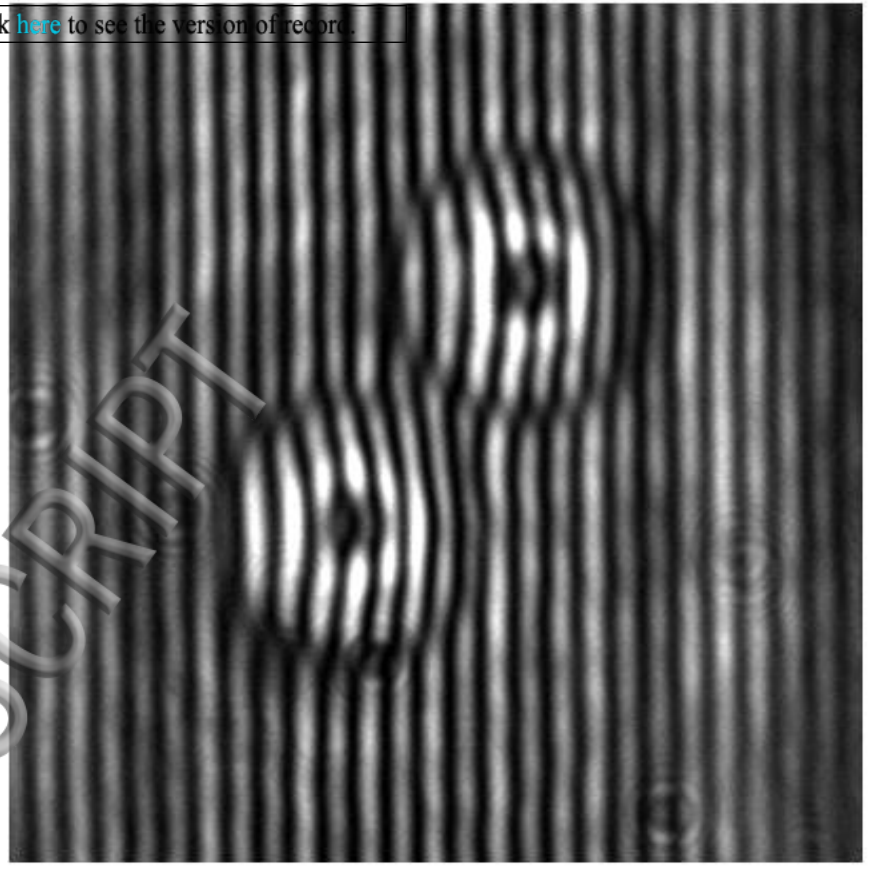

(b)

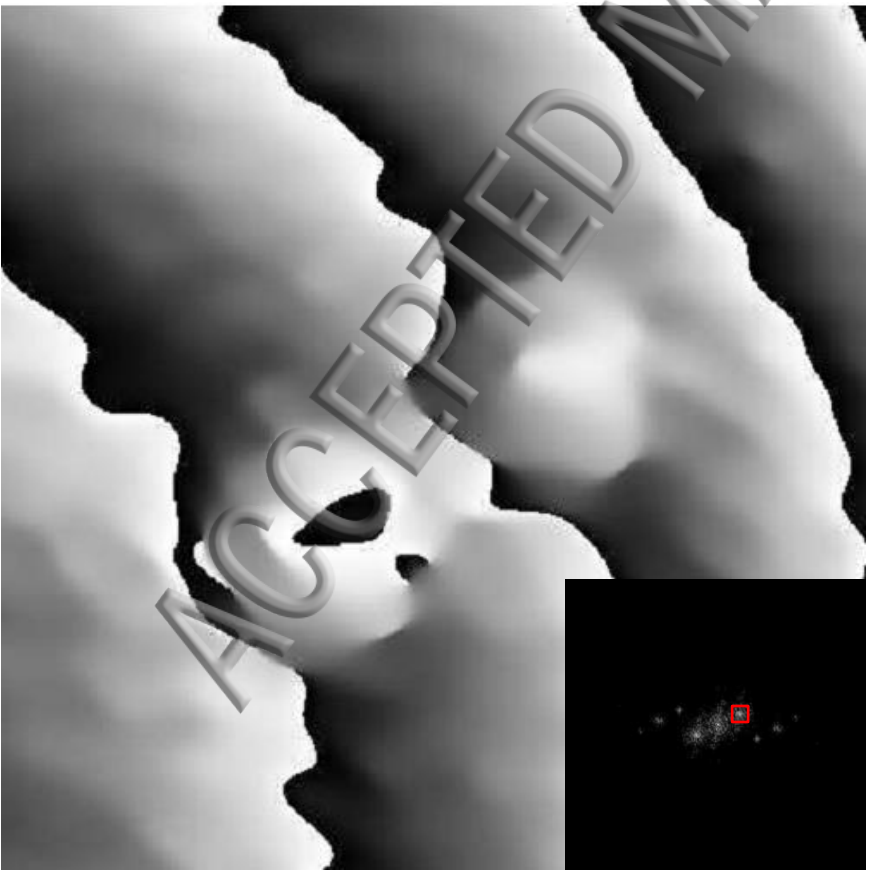

(c)

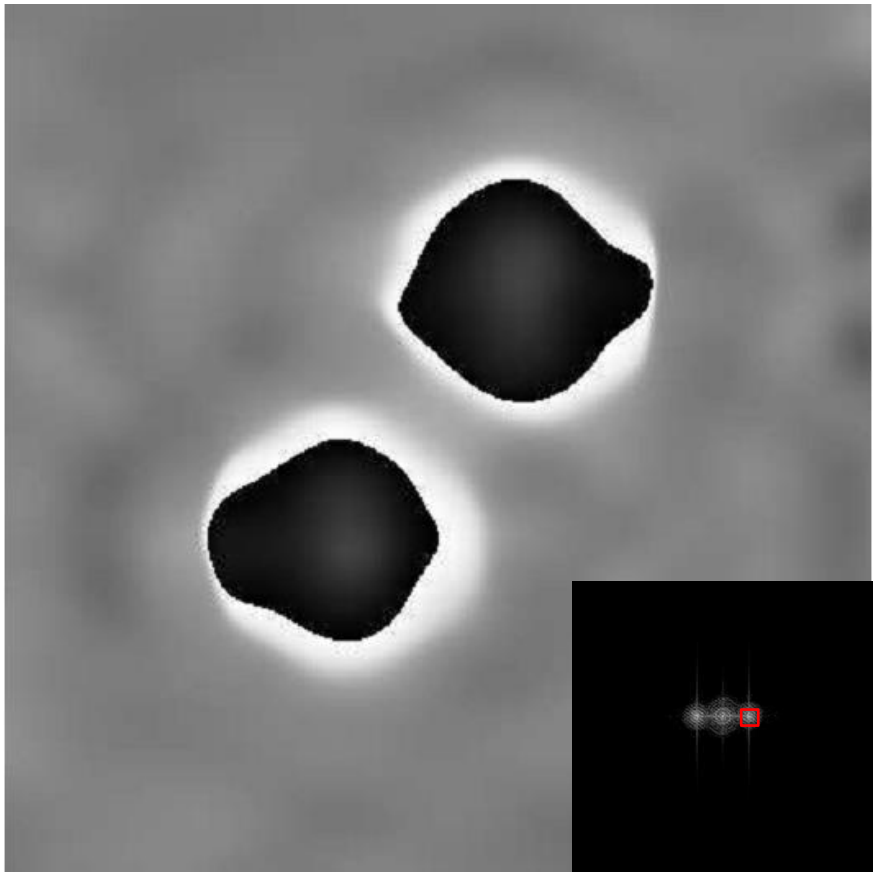

(d)

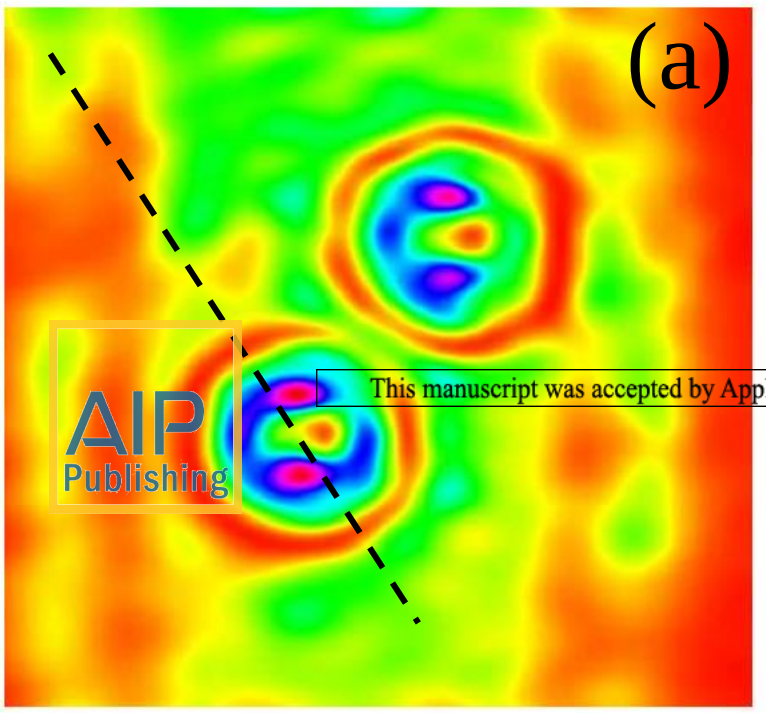

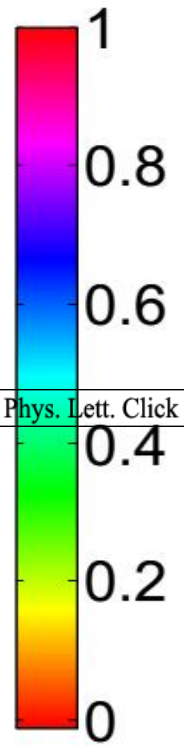

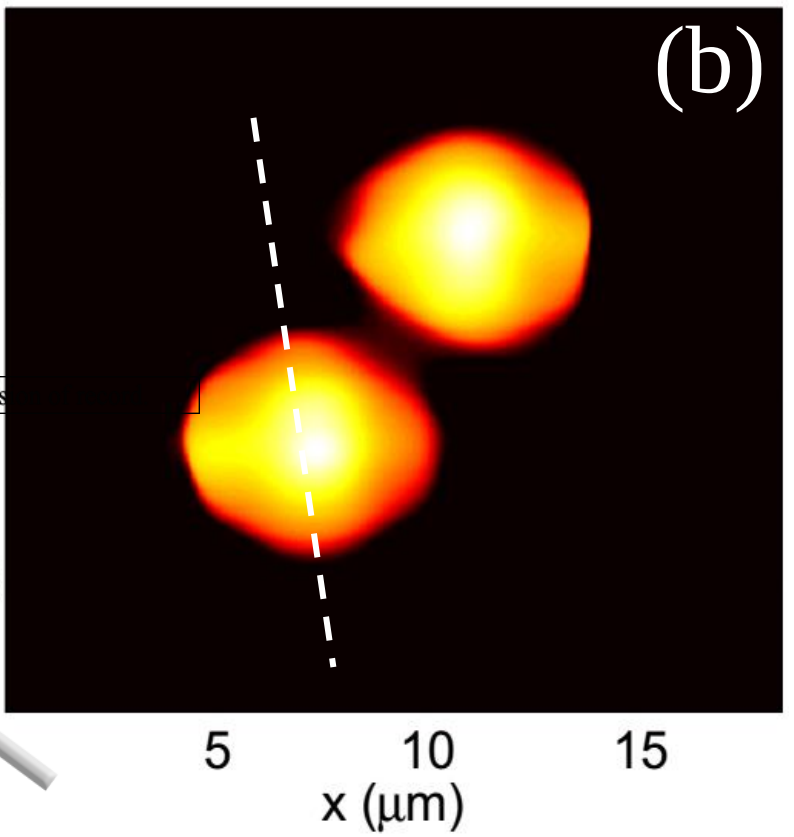

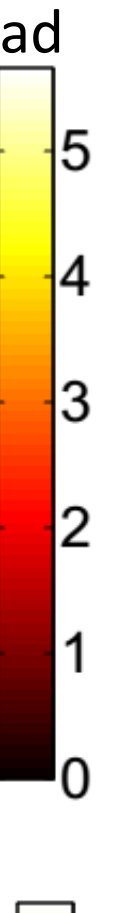

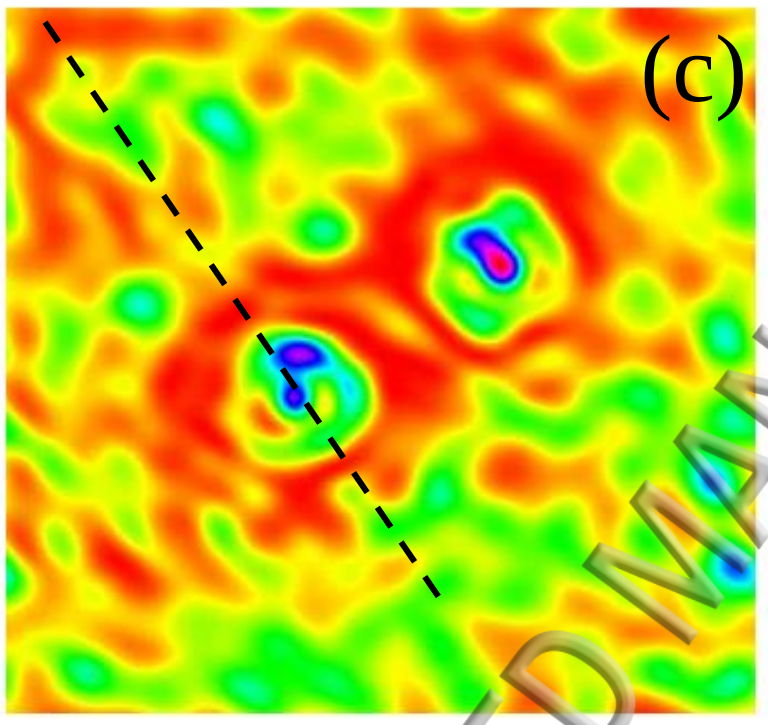

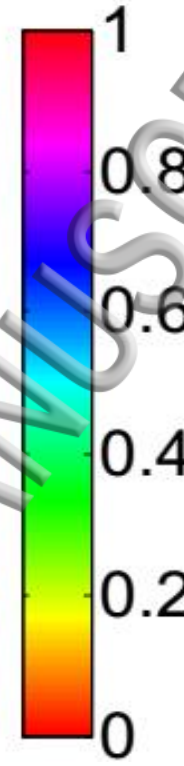

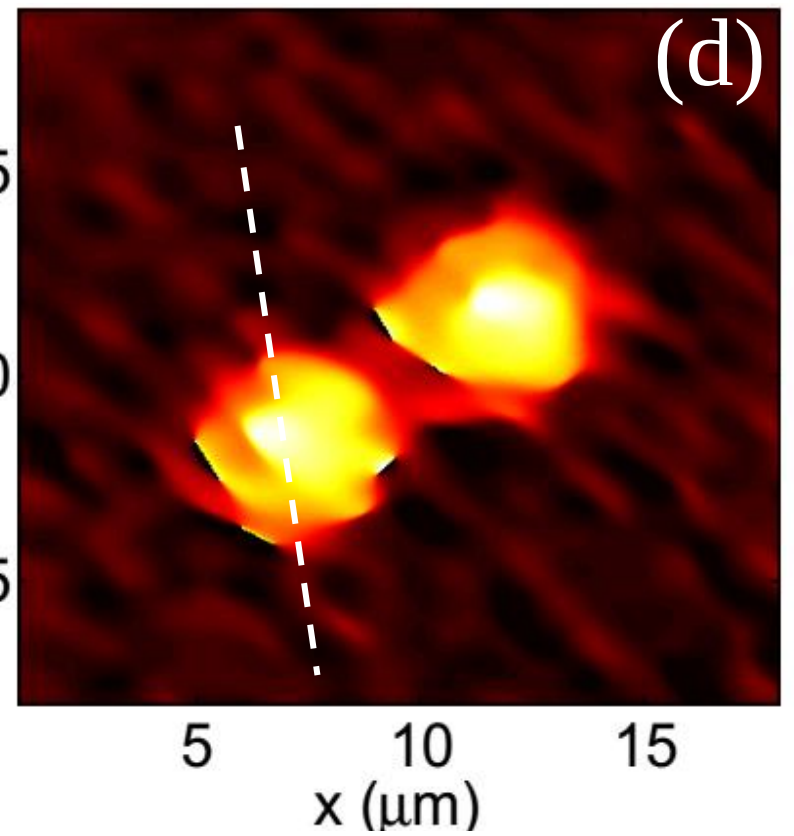

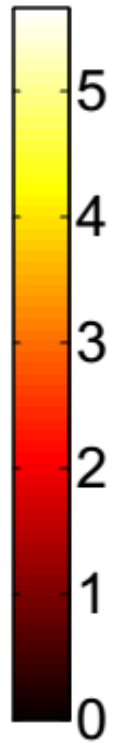

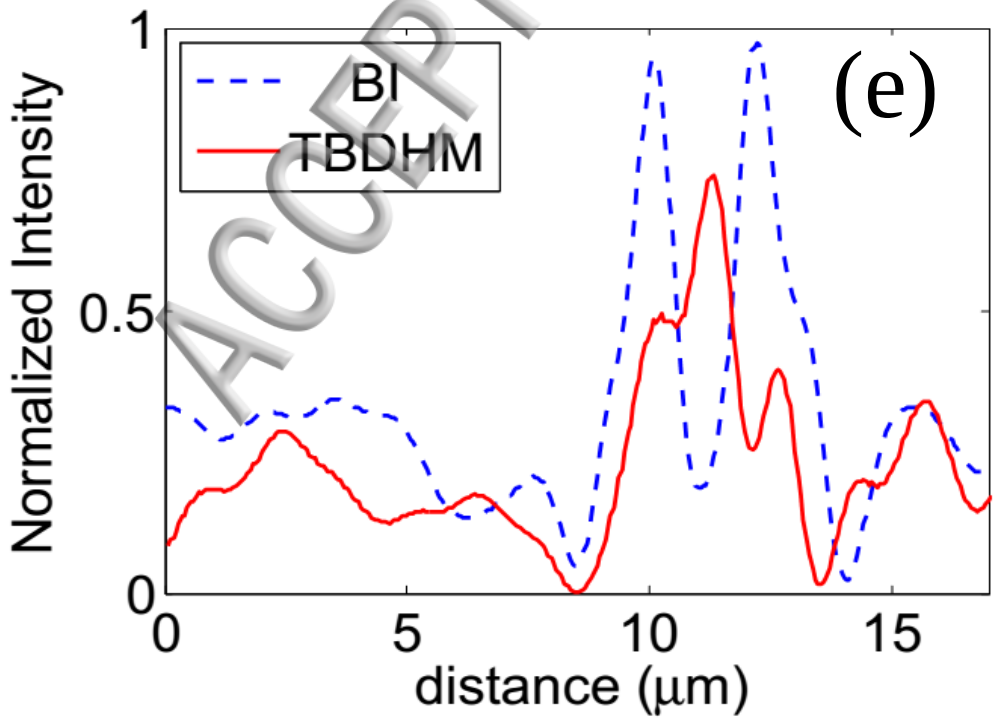

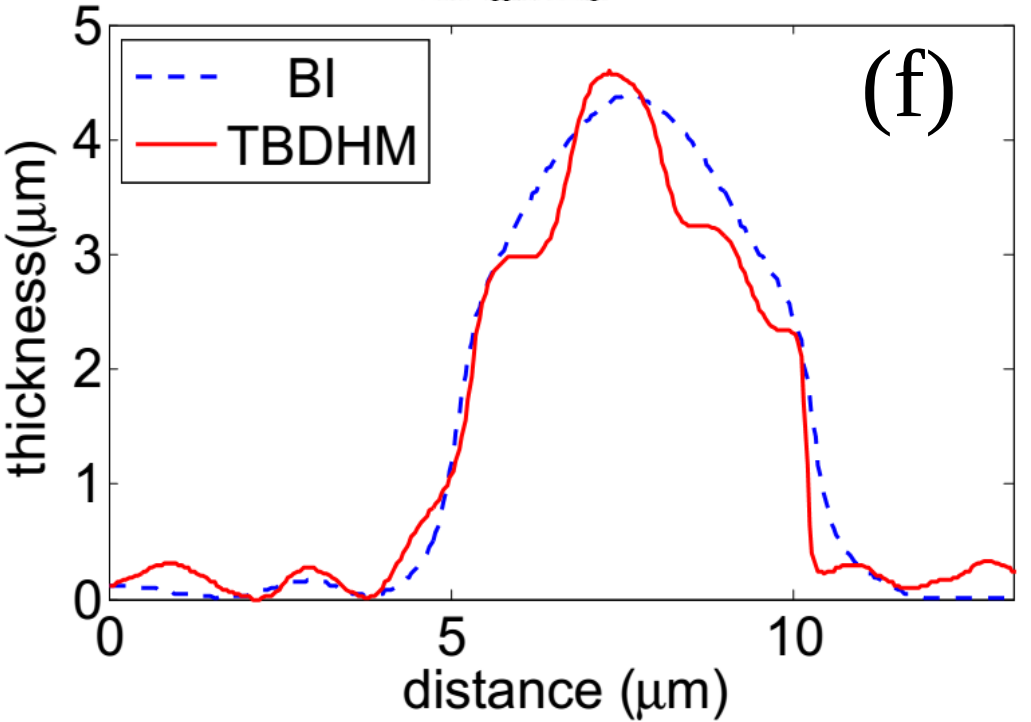

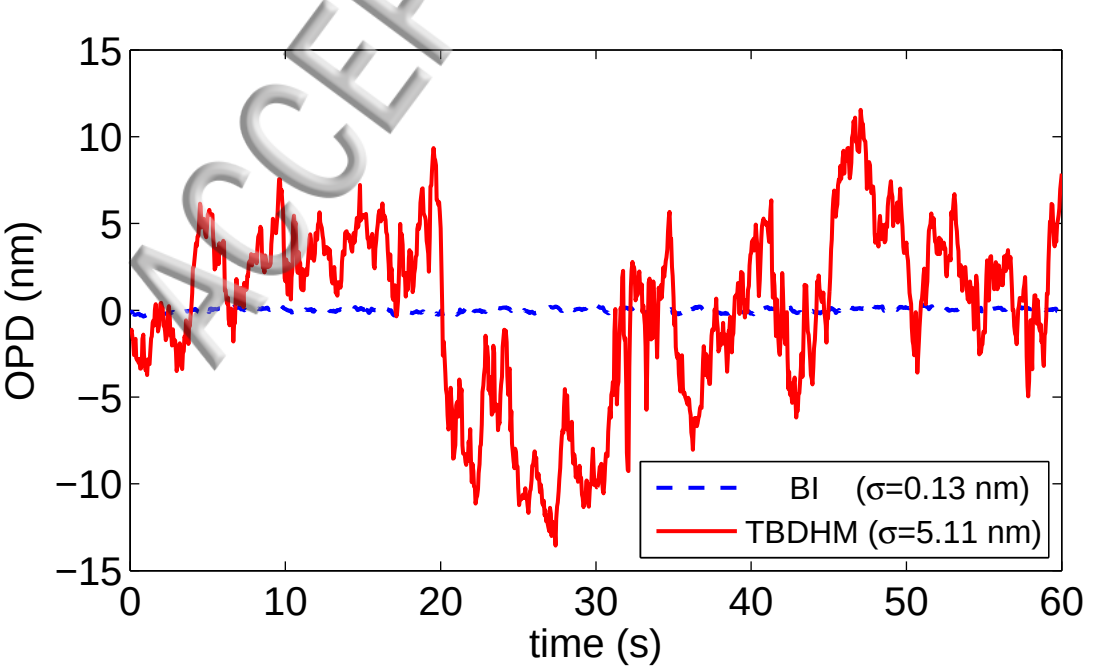
15
10
5
0
−5
−10
−15
OPD (nm)
0
10
20
30
40
50
60
time (s)
BI (σ=0.13 nm)
TBDHM (σ=5.11 nm)